BST2 regulated by the transcription factor STAT1 can promote metastasis, invasion and proliferation of oral squamous cell carcinoma via the AKT/ERK1/2 signaling pathway

FAYU SHAN[1], SI SHEN[1], XINXING WANG[2] and GANG CHEN[1]

[1]Department of Oral and Maxillofacial Surgery, School and Hospital of Stomatology, Tianjin Medical University, Tianjin 300070; [2]Environmental Medicine Laboratory, Tianjin Institute of Environmental and Operational Medicine, Tianjin 300050, P.R. China

Received November 1, 2022; Accepted February 22, 2023

DOI: 10.3892/ijo.2023.5502

Abstract. Oral squamous cell carcinoma (OSCC) is one of the main types of head and neck squamous cell carcinoma. Although progress has been made in treating OSCC, it remains a threat to human health, and novel therapeutic strategies are needed to extend the lifespan of patients with OSCC. The present study, evaluated whether bone marrow stromal antigen 2 (BST2) and STAT1 were potential therapeutic targets in OSCC. Small interfering RNA (siRNA) or overexpression plasmids were used to regulate BST2 or STAT1 expression. Western blotting and reverse transcription-quantitative PCR were performed to assess changes in the protein and mRNA expression levels of signaling pathway components. The effects of BST2 and STAT1 expression changes on the migration, invasion and proliferation of OSCC cells were assessed using the scratch test assay, Transwell assay and colony formation assay *in vitro*, respectively. Cell-derived xenograft models were used to evaluate the impact of BST2 and STAT1 on the occurrence and development of OSCC *in vivo*. Finally, it was demonstrated that BST2 expression was significantly upregulated in OSCC. Furthermore, it was demonstrated that high expression of BST2 in OSCC contributed to the metastasis, invasion and proliferation of OSCC cells. Moreover, it was demonstrated that the promoter region of BST2 was regulated by the transcription factor STAT1, and that the STAT1/BST2 axis could affect the behavior of OSCC via the AKT/ERK1/2 signaling pathway. *In vivo* studies also demonstrated that STAT1 down-regulation inhibited OSCC growth by down-regulating BST2 expression via the AKT/ERK1/2 signaling pathway.

Correspondence to: Dr Xinxing Wang, Environmental Medicine Laboratory, Tianjin Institute of Environmental and Operational Medicine, 1 Dali Road, Heping, Tianjin 300050, P.R. China
E-mail: wxxemail@sina.cn

Dr Gang Chen, Department of Oral and Maxillofacial Surgery, School and Hospital of Stomatology, Tianjin Medical University, 12 Qi Xinang Tai Road, Heping, Tianjin 300070, P.R. China
E-mail: doctorchen@tmu.edu.cn

Key words: STAT1/bone marrow stromal antigen 2, adenylate kinase 2/ERK1/2, oral squamous cell carcinoma

Introduction

Head and neck squamous cell carcinoma (HNSC) is a common cancer worldwide (1). It is estimated that there will be 139,170 new cases and 75,640 deaths associated with HNSC in China in 2022 (2). HNSC originates from the epithelial cells of the oral cavity, pharynx and larynx, and accounts for >90% of cancers in the head and neck region (3). Of all HNSC cases, ~25% are oral squamous cell carcinoma (OSCC) (4). The main risk factors for OSCC are smoking and drinking (5). Treatment for patients with early stage OSCC include surgery or radiation therapy, and for patients with advanced OSCC, multidisciplinary treatment strategies are required (6). However, the 5-year survival rate of patients with OSCC is <50% (7,8).

Bone marrow stromal antigen 2 (BST2) is an antiviral protein also known as tetherin, CD317 and HM1.24 (9). The main function of BST2 is to suppress the release of enveloped viruses by tethering the envelope of newly synthesized virions and binding them to the surface of cells (10). Much is known about the role of BST2 in immunity, but few previous studies have evaluated the role of BST2 in cancer, including its potential role in liver cancer (11) and breast cancer (12).

STAT1, a member of the STAT family of transcription factors, is the major mediator of the cellular response to interferons (IFNs) (13). However, the role of STAT1 in OSCC has not been previously elucidated.

Therefore, in the present study the regulation of the BST2 promoter by STAT1 was evaluated, and how this in turn affected the biological behavior (metastasis, invasion and proliferation) of OSCC was assessed.

Materials and methods

Bioinformatic analysis. The TCGA_HNSC tumor dataset from The Cancer Genome Atlas (portal.gdc.cancer.gov) and Genotype-Tissue Expression (ngdc.cncb.ac.cn) databases were

analyzed using the Gene Expression Profiling Interactive Analysis (GEPIA) database (gepia.cancer-pku.cn) and the linkedomics database (www.linkedomics.org). Briefly, expression levels of specific genes in different tumors were analyzed by methods such as the Gene Expression Profile and Gene Expression box plots. Kyoto Encyclopedia of Genes and Genomes (KEGG, www.linkedomics.org) signal pathway enrichment analysis of specific genes was performed using the linkedomics database.

The University of California Santa Cruz Genome Browser (UCSC; genome.ucsc.edu) and JASPAR (genome.ucsc.edu) databases were used to predict the transcription factors of BST2. Briefly, UCSC was used to predict transcription factors, and JASPAR was used to predict the specific sequences that transcription factors acted on.

Human oral squamous carcinoma cell lines and culture. SCC-15, SCC-25 and CAL-27 cell lines were cultured in DMEM (Gibco; Thermo Fisher Scientific, Inc.) with 10% fetal bovine serum (FBS; Invitrogen; Thermo Fisher Scientific, Inc.) and incubated at 37˚C with 5% CO_2. All cell lines were purchased from the American Type Culture Collection.

Small interfering RNA (siRNA) and plasmid transfection. SCC-15 cells ($1x10^5$ cells/well) were plated in 6-well plates. Using si-RNA Transmate Reagent (Suzhou GenePharm Co., Ltd.) the cells were transfected with negative control (NC) or siRNAs targeting BST2 or STAT1 (Table I). SiRNAs transfection was performed at 37˚C and the culture medium was replaced with fresh culture medium after 6 h. Follow-up procedures were performed 24 h later. Plasmid transfection for overexpression (oe-BST2; vector pcDNA3.1, NM_004335.4, 1.5 μg/well) or negative control (oe-NC; empty vector pcDNA3.1, 1.5 μg/well) was performed using Lipofectamine™ 3000 Reagent (Invitrogen; Thermo Fisher Scientific, Inc.) at 37˚C, and the culture medium was replaced 24 h later and subsequent treatment were performed. The siRNA sequences and plasmids were purchased from Suzhou GenePharm Co. Ltd.

RNA extraction and reverse transcription-quantitative (RT-q) PCR. The total RNA of a cell or tissue was extracted using a UNIQ-10 Column Trizol Total RNA Isolation Kit (Sangon Biotech Co., Ltd.), and complementary DNA was generated using PrimeScript RT Master Mix (Takara Bio, Inc.) and PCR Veriti thermocycler (Thermo Fisher Scientific, Inc.). The thermocycling conditions used were as follows: 37˚C for 15 min, 85˚C for 5 sec and were then cooled to 4˚C upon completion. Quantitative PCR assays were performed using a A28134 QuantStudio® 5 Real-Time PCR Instrument (Thermo Fisher Scientific, Inc.) and iTaq Universal SYBR Green Supermixi reagent (Bio-Rad Laboratories, Inc.) in 8 Strip Real-time PCR Tubes (Sangon Biotech Co., Ltd.). The sequences of the primers (Sangon Biotech Co., Ltd.) used were presented in Table II. The thermocycling conditions used were as follows: 95˚C for 30 sec, 40 cycles of 95˚C for 3 sec and 60˚C for 30 sec, then 60˚C for 20 sec and 95˚C for 1 sec. The relative expression of each gene was calculated using the $2^{-\Delta\Delta Cq}$ method with β-actin as the internal reference (14). The primer sequences were purchased from Suzhou GenePharm Co. Ltd.

Cell proliferation assay with Cell Counting Kit-8 (CCK-8). Briefly, 1,000 SCC-15 cells were plated in 96-well plates in 100 μl DMEM (Gibco; Thermo Fisher Scientific, Inc.) with 10% FBS (Invigentech Inc.). The cells were cultured for 24, 48 and 72 h. The CCK-8 stock solution (Dojindo, Japan) was diluted 1:10 with 100% DMEM, serum-free medium (Gibco; Thermo Fisher Scientific). The original medium was removed and the assay reagents were added to the well. After the cells were incubated for 1.5 h, results were assessed as the OD 450 nm on a SpectraMax M5 microplate reader (Molecular Devices, LLC.).

Scratch test assay. Transfected or untreated SCC-15 cells ($8x10^5$ cells/well) were cultured to ~100% confluence. The cells were scratched with a 1 ml pipette tip. Cells that were floating in suspension were removed using PBS. The cells were cultured in serum-free medium at 37˚C for 48 h. The cells were imaged using a DMi8 light microscope (Leica Microsystems GmbH). ImageJ (version 1.8.0.345; National Institutes of Health) was used to assess the micrographs.

Transwell cell invasion assay. Transfected or untreated SCC-15 cells ($5x10^4$/well, 200 μl) were plated in the upper chamber of the Transwell insert (8 μm/pore; cat. no. 354480; Corning, Inc.) with serum-free DMEM (Gibco; Thermo Fisher Scientific), and the chamber was placed in a well containing 600 μl DMEM (Gibco; Thermo Fisher Scientific) with 20% FBS. The cells were incubated at 37˚C for 48 h. The Transwell chambers were supplied pre-treated with Matrigel the chamber to assess the invasion ability of the cells. Finally, after removing cells from the wells, cells in the lower chamber were fixed using 4% formalin at room temperature for 15 min. The cells were washed with PBS and stained with 1x Giemsa Staining Solution (Beijing Solarbio Science & Technology Co., Ltd.) at room temperature for 30 min. The final results were imaged using a DMi8 light microscope (Leica Microsystems GmbH). ImageJ (version 1.8.0.345; National Institutes of Health) was used to assess the micrographs.

Clone formation assay. Following transfection, SCC-15 cells ($1x10^4$ cells/ml) were plated into 60 mm-dishes and incubated for 10 days at 37˚C. Then, the cells were fixed using 4% formaldehyde at room temperature for 15 min and stained with 1x Giemsa Staining Solution (Beijing Solarbio Science & Technology Co., Ltd.) for 30 min. The size of cloned cell colonies was quantified using ImageJ (version 1.8.0.345; National Institutes of Health).

Dual-luciferase reporter assay. SCC-15 cells (80% confluence) were co-transfected with BST-wild-type (WT; TTT CTGGGAAA; 50 ng) or BST2-mutant (MUT; CCGACT TAGGC; 50 ng) and oe-STAT1 (1.5 μg, vector pcDNA3.1, NM_007315.4) or oe-NC (1.5 μg, empty vector pcDNA3.1) using Lipofectamine 3000 (Invitrogen; Thermo Fisher Scientific, Inc.), according to the aforementioned method. After 48 h of incubation, the luciferase activity was evaluated using the Dual Luciferase Reporter Gene Assay Kit (cat. no. KGAF040; Nanjing KeyGen Biotech Co., Ltd.). The results were analyzed using a SpectraMax M5 microplate reader (Molecular Devices, LLC.) with *Renilla* luciferase activity as

Table I. si-RNA sequences.

Target	Sequence (5'-3')
STAT1	S: GCGUAAUCUUCAGGAUAAUTT
	A: AUUAUCCUGAAGAUUACGCTT
BST2	S: GCAAUGUCACCCAUCUCCUTT
	A: AGGAGAUGGGUGACAUUGCTT
Negative control	S: UUCUCCGAACGUGUCACGUTT
	A: ACGUGACACGUUCGGAGAATT

S, sense; A, antisense; BST2, bone marrow stromal antigen 2.

Table II. Sequences of primers used for reverse transcription-quantitative PCR.

Gene	Sequence (5'-3')
STAT1	F: GTTTGTGGTGGAAAGACAGCC
	R: TCTCTCATTCACATCTCTCAACTT
BST2	F: CTGGGGGTGCCCTTGATTAT
	R: AGCCATTAGGGCCATCACAGT
β-actin	F: CATGTACGTTGCTATCCAGGC
	R: CTCCTTAATGTCACGCACGAT

F, forward; R, reverse; BST2, bone marrow stromal antigen 2.

the internal reference. The WT, MUT BST2, the STAT1 overexpression plasmid and the luciferase reporter plasmid were purchased from Nanjing KeyGen Biotech Co., Ltd.

Western blotting. Transfected cells were washed and incubated in RIPA with PMSF (100:1) for at 4˚C for 30 min. The lysate was centrifuged at 10,000 x g at 4˚C for 10 min and precipitates were removed. The protein concentration was measured using a BCA Protein Assay Kit (Beijing Solarbio Science & Technology Co., Ltd.). The proteins (20 μg/lane) were separated using SDS-PAGE electrophoresis in 4 to 20% polyacrylamide gels and transferred to PVDF membranes (Invitrogen; Thermo Fisher Scientific, Inc.). The PVDF containing protein membranes were blocked in 5% skim milk at room temperature for 120 min. The membranes were then incubated overnight with primary antibodies against STAT1 (1:1,000; cat. no. 10144-2-AP; ProteinTech Group, Inc.), phosphorylated (p)-STAT1 (1:1,000; cat. no. ab109461; Abcam), AKT (pan; 1:1,000; cat. no. 4691S; Cell Signaling Technology, Inc.), p-AKT (1:2,000; cat. no. 4060S; Cell Signaling Technology, Inc.), ERK1/2 (1:1,000; cat. no. 11257-1-AP; ProteinTech Group, Inc.), p-ERK1/2 (1:1,000; cat. no. 28733-1-AP-ProteinTech Group, Inc.) or β-actin (1:2,000; cat. no. 20536-1-AP; ProteinTech Group, Inc.) at 4˚C. Membranes were then washed with TBST with 0.1% Tween and incubated with Goat anti-rabbit IgG (H&L) secondary antibodies (1:10,000; cat. no. bs13278; Bioworld Technology, Inc.) at 25˚C for 1 h. The protein bands were visualized using an Amersham Imager 680 (Cytiva) with ECL (cat. no. WBKLS0500; MilliporeSigma). The relative expression of each protein was calculated using ImageJ (version 1.8.0.345; National Institutes of Health) with β-actin as an internal reference.

Lentiviral transduction. The plasmids and reagents used in the manufacture of Lentivirus-RNA interference-STAT1 (Levi-RNAi-STAT1) were purchased from Suzhou GenePharma Co., Ltd. Briefly, lentivirus-RNAi was produced using a second generation system and 293T cells were used as the interim cells. The 293T cells were purchased from the American Type Culture Collection. A total of 20 μg GV vector plasmid, 15 μg pHelper 1.0 vector plasmid and 10 μg pHelper 2.0 vector plasmid were transfected into 293T cells and cultured at 37˚C for 6 h. After 6 h, the old culture medium was replaced with fresh culture medium and incubation was continued at 37˚C for 48 h. The supernatant was then collected and centrifuged at 4˚C and 4,000 x g for 10 min. The supernatant was discarded, PBS added, and then centrifuged at 10,000 x g at 4˚C for 5 min. The supernatant was then collected and used as the virus stock solution ($1x10^8$ TU/ml). The MOI value (MOI=50) was determined according to the manufacturer's protocol. The target SCC15 cells ($1x10^4$ cells/well) were plated in a 6-well plate and incubated at 37˚C for 24 h. The virus stock solution was diluted and added to the six-well plate. The cells were cultured at 37˚C for 12 h. Culture medium was replaced with fresh medium 12 h after transduction. Transfected cells were screened for 3 days at 1 μg/ml purinomycin at 37˚C and then screened for a further 48 h at 0.5 μg/μl purinomycin at 37˚C to obtain cells with STAT1-downregulated. STAT1-downregulated expression cells were kept in 0.25 μg/μl purinomycin for maintenance. The STAT1-downregulated express cell strains obtained through the above steps were then used in *in vivo* experiments. The lentiviral-encapsulated si-RNA sequences were presented in Table I.

In vivo tumor model. All animal studies were approved by the Tianjin Institute of Environmental and Operational Medicine Experimental Animal Ethics Committee (approval no. IACUC of AMMS-04-2022-018). Female athymic mice (n=24; age, 5 weeks; weight, 17-20 g) were randomly divided into three groups as follows: i) control group (n=8, SCC-15 cells), ii) Levi-RNAi-siNC group (n=8, SCC-15 cells transfected with RNAi-NC lentivirus), and iii) Levi-RNAi-siSTAT1 group (n=8, SCC-15 cells transfected with RNAi-STAT1 lentivirus). A total of 100 μl of cells in PBS ($5x10^7$ cells/ml) were injected subcutaneously into dorsal skin of mice ($5x10^6$ cells/mouse). The tumor volume was measured every three days once the tumors were visible (volume=length/2 x width^2). The animal experiment was terminated when the tumor volume in the control group reached ~1,500 mm^3 or signs of decreased mobility, self-harm or necrosis were observed. The mice were euthanized with CO_2 (60% displacement of cage volume/min). Subcutaneous tumor tissues and other tissues were collected after the absence of a heartbeat and spontaneous breathing for 15 min. Finally, three mice were randomly selected and their tumors were collected for western blotting, RT-qPCR, hematoxylin and eosin (H&E) staining and immunohistochemical (IHC) staining experiments.

IHC analysis. Lung, heart, liver and tumor tissues were collected from cell-derived xenograft (CDX) models. Tissues were washed with normal saline and immediately fixed in 4% paraformaldehyde at room temperature for 24 h. Tissues were cut into 5 μm sections. The paraffin-embedded sections were dewaxed at 58˚C and put it into dimethylbenzene for 10 min, 100% alcohol for 5 min, 95% alcohol for 5 min and then 75% alcohol for 5 min at room temperature for rehydration, and then washed with water and placed in water to prepare for antigen retrieval. The antigen retrieval solution (EDTA) was added to a pressure cooker and heated to a boil using an induction cooker. The dewaxed and hydrated tissue sections were placed in boiling EDTA for 1.5 min before being removed and cooled naturally to room temperature. Sections were then washed three times with PBS. The sections were soaked in 3% H_2O_2 for 30 min, and were then washed three times with PBS.

The sections were soaked in PBS with 10% Tween at room temperature for 3 min and then blocked using 100% goat serum (cat. no. AR1009; Wuhan Boster Biological Technology, Ltd., Wuhan, China.) at 25˚C for 30 min. The serum on the sections was removed and sections were incubated at 37˚C for 1 h with primary antibodies as follows: STAT1 (1:900; cat. no. 10144-2-AP; ProteinTech Group, Inc.); p-STAT1 (1:900; cat.no. ab109461; Abcam); BST2 (1:900; cat.no. 13560-1-AP; ProteinTech Group, Inc.). Sections were then rinsed with PBS and then rinsed three times with water. The sections were then soaked and rinsed in PBS with 10% Tween three times. Sections were then incubated with Goat anti-rabbit IgG (H&L) secondary antibodies (1:2,000; cat. no. ab205718; Abcam) for 45 min at 37˚C. Then DAB was added to allow assessment of the color development under the microscope. After color development, the reaction was terminated with water and the sections were soaked. Then, hematoxylin dye solution was added at room temperature for 2 min, and then rinsed with distilled water, and the color separation solution (cat. no. BP022, BIOSSCI) was added, then rinsed with water three times. The slides were sequentially dehydrated in 100% absolute ethanol at 25˚C for 10 sec. A charge-coupled device light microscope was used for assessment and imaging of the section.

H&E staining. Lung, heart, liver and tumor tissues obtained from the CDX model were made into sections according to the aforementioned method in the immunohistochemical analysis section. The sections were dewaxed in dimethylbenzene for 5 min and dehydrated in 100, 95, 85 and 75% alcohol for 5 min, respectively. After that, the sections were stained with hematoxylin for 5 min and differentiated with 1% hydrochloric acid alcohol for 5 sec. Sections were then stained with eosin for 15 sec and dehydrated in 95 and 100% alcohol for 1 min each, before clearing with dimethylbenzene for 5 min. Subsequently, the sections were fixed using neutral balsam. All stages of H&E staining were performed at 25˚C. Finally, the sections were imaged using a DMi8 light microscope (Leica Microsystems GmbH).

Statistical analysis. Data were collected from three independent experiments and GraphPad Prism 9 (GraphPad Software; Dotmatics) was used for data analysis. Data were presented as the mean ± SD. Unpaired Student's t-test was used to analyze differences between groups and one-way analysis of variance with Tukey's post-hoc test was used to analyze multiple groups. $P<0.05$ considered to indicate a statistically significant difference.

Results

BST2 is highly expressed in HNSC and OSCC cell lines. The GEPIA database was used to analyze the expression levels of BST2 in HNSC. The BST2 expression levels in HNSC were markedly abnormally elevated (Fig. 1A). KEGG pathways were analyzed using the linkedomics database (15). BST2 was enriched in immune-related pathways, which may be a reason which has limited the number of studies on BST2 in cancer (Fig. 1C). GEPIA was also used to analyze BST2 expression in tumor and normal tissues. The results showed that the expression of BST2 in tumor tissues was significantly higher than that in normal tissues. (Fig. 1B). BST2 mRNA and protein expression levels in different cell lines was analyzed by RT-qPCR and western blotting, respectively. The expression level of BST2 in SCC15 cell line was statistically different from that in the CAL27 cell line, while there was no significant statistical difference between BST2 and SCC15 (Fig. 1D). Based on bioinformatic analysis, BST2 was highly expressed in HNSC compared with other types of tumor. Moreover, western blotting and RT-qPCR experiments demonstrated that the protein and mRNA expression levels of BST2 in the SCC-15 cell line were markedly higher than those in the SCC-25 and CAL-27 cell lines. Therefore, the SCC-15 cell line was selected for use in subsequent experiments.

BST2 downregulation suppresses migration, invasion, and proliferation of OSCC cells. SCC-15 cells were transfected with siRNA targeting BST2, and the efficiency of BST2 gene downregulation was evaluated using western blotting and RT-qPCR, which demonstrated a significant downregulation efficiency (Fig. 2A). Furthermore, scratch test assays, Transwell cell invasion assays and clone formation assays were used to evaluate changes in the biological behavior after BST2 downregulation. The results demonstrated that the migration, invasion and proliferation ability of SCC-15 cells was significantly decreased after BST2 downregulation (Fig. 2B-E).

BST2 overexpression increases migration, invasion, and proliferation of OSCC cells. To further evaluate the role of BST2 in OSCC, a BST2 overexpression plasmid was constructed and the effects of BST2 overexpression on the migration, invasion and proliferation of OSCC were assessed. Western blotting and RT-qPCR were used to verify the overexpression efficiency, which demonstrated significant overexpression of BST2 (Fig. 3A). Moreover, it was demonstrated that the proliferation ability of OSCC was significantly increased after overexpression of BST2 via scratch test assays, Transwell cell invasion assays and clone formation assay (Fig. 3B-E). These data suggest that BST2 serves a role in promoting tumor growth in OSCC.

STAT1 binds to the BST2 promoter to activate BST2 expression in OSCC. Proteomics databases, including the JASPAR and UCSC databases, were used to predict the binding sites between STAT1 and BST2 (Fig. 4A). In SCC-15 cells

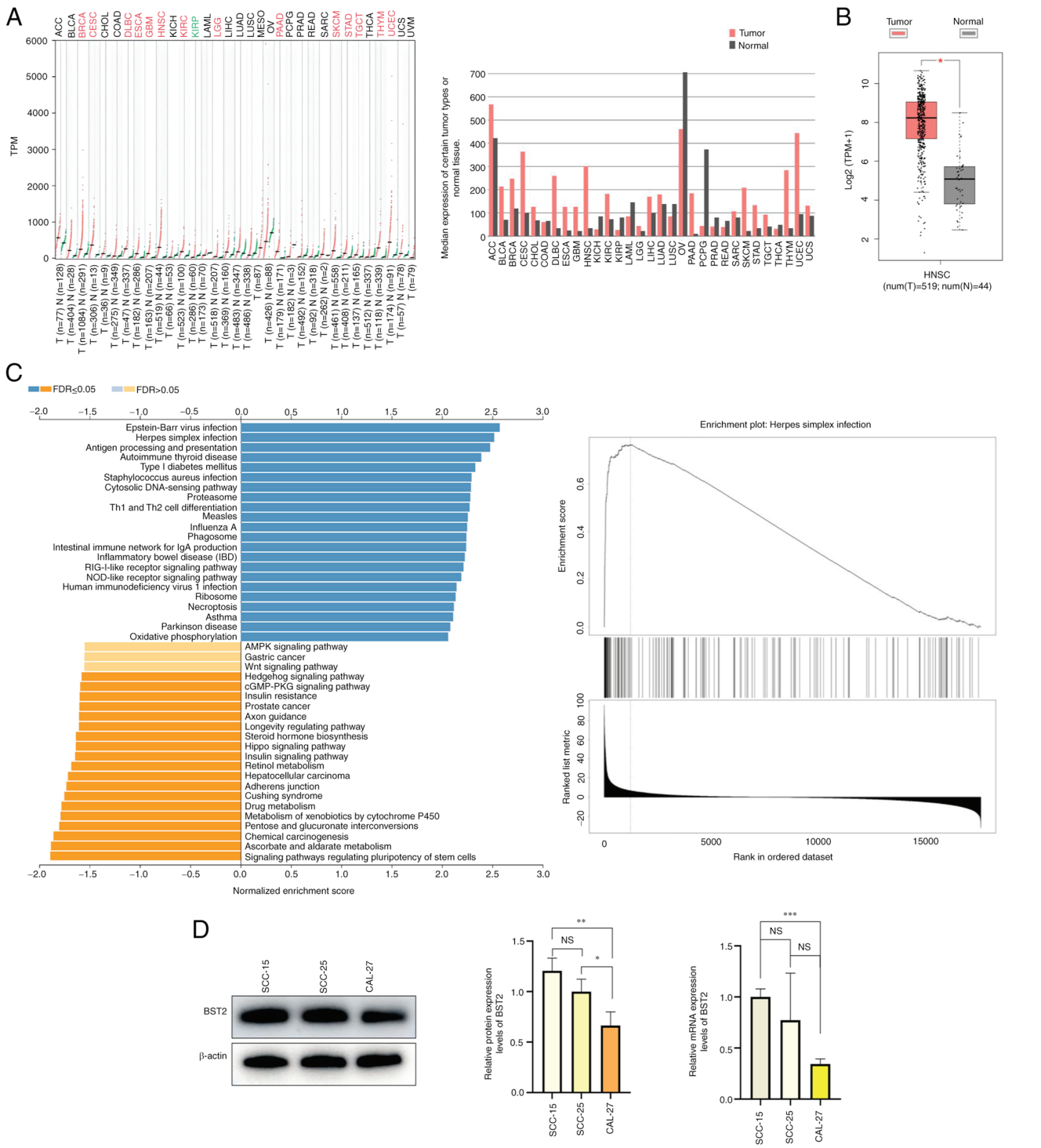

Figure 1. BST2 is highly expressed in HNSC and OSCC cell lines. (A) The mRNA expression levels of BST2 in different tumor types from the Gene Expression Profiling Interactive Analysis database (B) Differential expression of BST2 between normal and tumor tissue (tumor tissues, n=519; normal tissues, n=44). (C) Kyoto Encyclopedia of Genes and Genomes pathway analysis performed by linkedomics database. (D) The protein and mRNA expression levels of BST2 in different OSCC cell lines. *P<0.05, **P<0.01 and ***P<0.001. HNSC, head and neck squamous cell carcinoma; OSCC, oral squamous cell carcinoma; TPM, transcripts per million; FDR, false discovery rate; BST2, bone marrow stromal antigen 2; NS, not significant; T, tumor; N, normal.

transfected with si-STAT1, the mRNA expression levels of STAT1 and BST2 were significantly downregulated compared with si-NC groups (Fig. 4B). However, after overexpression or downregulation of BST2, STAT1 mRNA levels were not significantly different compared with the control group. Furthermore, results of the dual-luciferase reporter assay demonstrated that relative luciferase activity was significantly increased in SCC-15 cells co-transfected with BST2-WT promoter reporter and oe-STAT1 compared with the BST2-WT promoter reporter and oe-NC (Fig. 4C). Which suggested that the transcription factor STAT1 may regulate BST2 in OSCC. These data demonstrated, for the first time using the dual-luciferase reporter assay, that STAT1 could regulate BST2 through regulation of its specific promoter sequence.

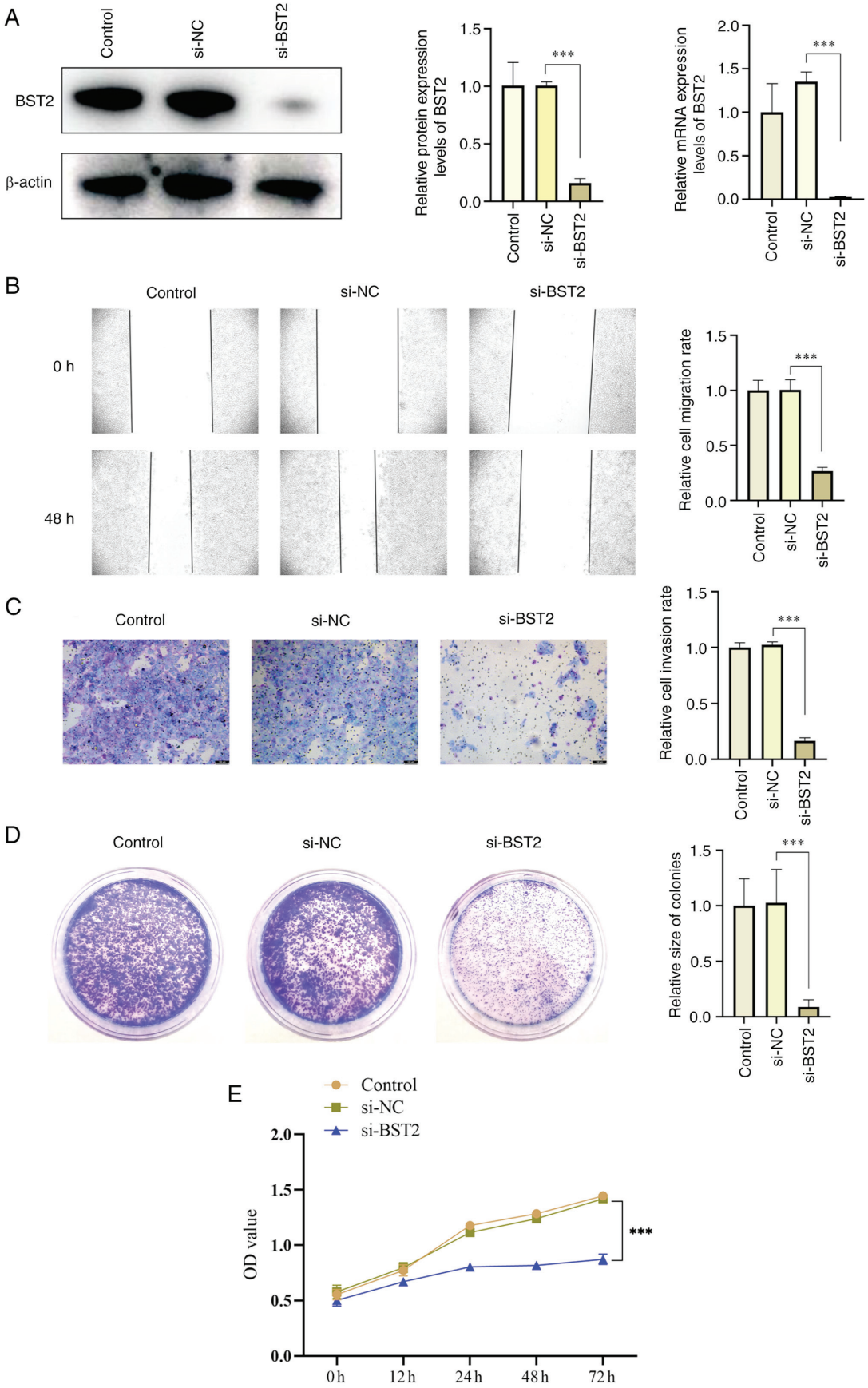

Figure 2. BST2 downregulation suppresses oral squamous cell carcinoma cell migration, invasion and proliferation. (A) Western blotting and reverse transcription-quantitative PCR analysis of the protein and mRNA expression levels of BST2, respectively, after BST2 downregulation using si-RNA in SCC-15 cells. (B) Cell scratch test assay (magnification x50), and (C) Transwell assay (magnification, x100) were used to assess the migration and invasion ability of SCC-15 cells after BST2 downregulation using siRNA. (D) Clone formation and (E) cell proliferation assays were performed to evaluate changes in the viability and proliferation of SCC-15 cells after BST2 downregulation. ***P<0.001. BST2, bone marrow stromal antigen 2; si, small interfering; NC, negative control.

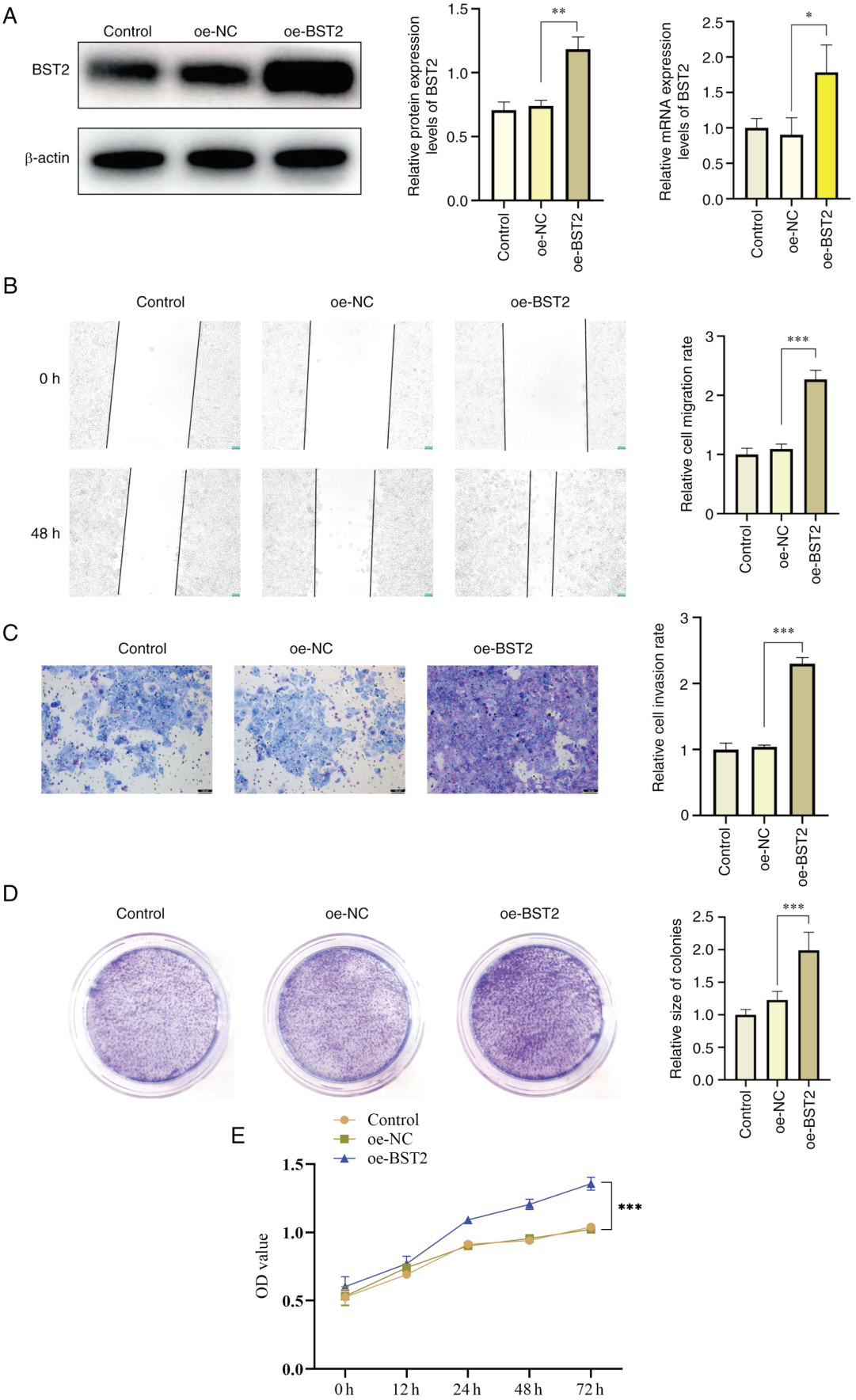

Figure 3. BST2 overexpression enhances OSCC cell migration, invasion and proliferation. (A) Western blotting and reverse transcription-quantitative PCR analysis of the protein and mRNA expression levels of BST2 after BST2 overexpression using an overexpression plasmid in SCC-15 cells. (B) Cell scratch test assay (magnification, x50), and (C) Transwell assay (magnification, x100) were used to assess the migration and invasion ability of SCC-15 cells after BST2 overexpression. (D) Clone formation and (E) cell proliferation assays were performed to assess changes in the viability and proliferation of SCC-15 cells after BST2 overexpression. *P<0.05, **P<0.01 and ***P<0.001. BST2, bone marrow stromal antigen 2; oe, overexpression; NC, negative control.

A

Matrix ID	Name	Score	Relative score	Predicted sequence
MA0137.3	MA0137.3.STAT1	17.0403	0.9932	TTTCTGGGAAA

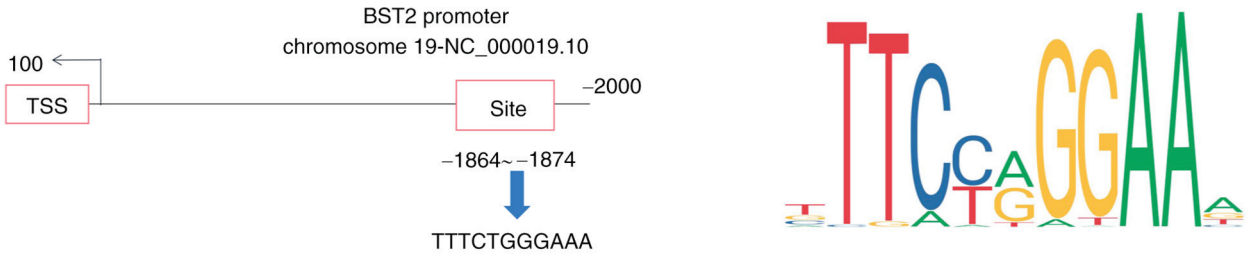

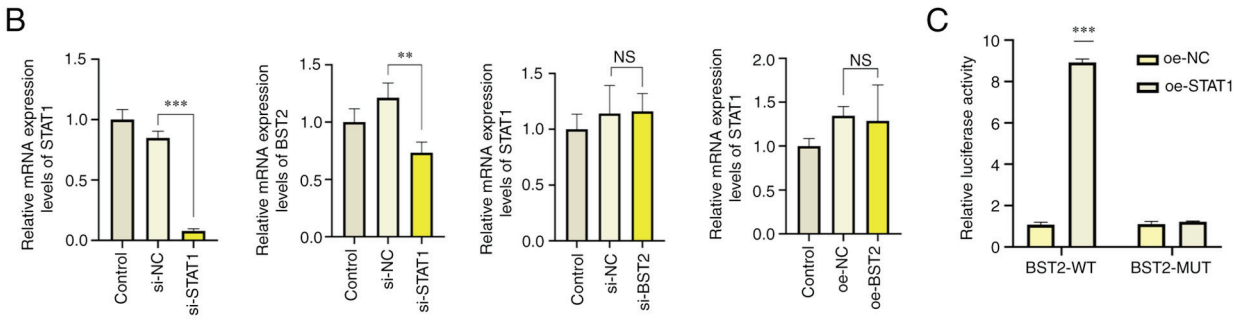

Figure 4. STAT1 binds to the BST2 promoter to regulate BST2 expression in oral squamous cell carcinoma. (A) JASPAR and UCSC databases were used to predict the binding sites between STAT1 and the BST2 promoter. (B) mRNA expression levels of STAT1 and BST2 in SCC-15 cell lines were assessed using reverse transcription-quantitative PCR after regulation of STAT1 or BST2. (C) Relative luciferase activity was assessed using the dual-luciferase reporter assay in SCC-15 cells co-transfected with oe-STAT1 or oe-NC and BST2-WT or BST2-MUT. **P<0.01 and ***P<0.001. BST2, bone marrow stromal antigen 2; oe, overexpression; WT, wildtype; MUT, mutant; NS, not significant; UCSC, University of California Santa Cruz Genome Browser.

STAT1 is upregulated in HNSC and OSCC cell lines. The GEPIA database was used to analyze STAT1 expression in a panel of cancers. The expression level of STAT1 in HNSC was markedly higher compared with other tumor types (Fig. 5A). The linkedomics database was used to perform KEGG analysis on STAT1, which demonstrated that STAT1 was enriched in immune-related pathways. In previous studies, bioinformatics analysis of BST2 has focused on immunity (41), which has resulted in BST2 being poorly studied in tumors, this may be one of the reasons limiting studies on STAT1 in OSCC. (Fig. 5C). STAT1 expression was significantly increased in OSCC (Fig. 5B). Western blotting and RT-qPCR were used to assess STAT1 protein and mRNA expression levels, respectively, in SCC-15, SCC-25 and CAL-27 OSCC cell lines (Fig. 5D). The above bioinformatics analysis indicated that both STAT1 and BST2 were highly expressed in OSCC and suggested that there may be a functional relationship between STAT1 and BST2 in OSCC.

STAT1 positively regulates BST2/AKT/ERK1/2 pathway facilitates migration, invasion, and proliferation of OSCC cells. To further assess the relationship between STAT1 and BST2 and to elucidate the downstream pathways involved, si-RNA was used to down-regulate STAT1 and BST2 expression and overexpression plasmids were used to up-regulate BST2 expression. Western blotting demonstrated that BST2 protein expression levels decreased significantly following si-RNA downregulation of STAT1, whereas STAT1 phosphorylation and STAT1 protein expression levels did not significantly change after overexpression or silencing of BST2 (Fig. 6A). This further indicated that STAT1 regulated BST2 expression in OSCC. Moreover, the downstream pathway of BST2 was evaluated. Western blotting demonstrated that the activity of the AKT/ERK1/2 signaling pathway significantly increased when BST2 was up-regulated and significantly decreased when BST2 was down-regulated. When STAT1 was silenced, the BST2/AKT/ERK1/2 signaling pathway was also down-regulated (Fig. 6A). This indicated that BST2 activated the AKT/ERK1/2 signaling pathway in OSCC.

Similarly, scratch test assays, Transwell cell invasion assays and clone formation assays were used to assess the effects of STAT1 on migration, invasion and proliferation of OSCC cells. The results demonstrated that the proliferation, migration and invasion of si-STAT1 OSCC cells was significantly decreased compared with si-NC OSCC cells (Fig. 6B-E). These data suggested that STAT1 and BST2 serve a synergistic role in OSCC.

STAT1 and BST2 serve a synergistic role in the biological behavior of OSCC. si-RNA and plasmids were used to co-transfect SCC-15 cells to further evaluate the relationship between STAT1 and BST2, and the AKT/ERK1/2 signaling pathway. Compared with the si-NC group, the BST2/AKT/ERK1/2 signaling pathway was markedly inhibited after down-regulation of STAT1. However, when BST2 was upregulated simultaneously with STAT1 downregulation, the activation of the BST2/AKT/ERK1/2 signaling pathway was rescued (Fig. 7A). Furthermore, similar results were demonstrated in the cell scratch test assay, Transwell assay and proliferation assay, namely that the inhibitory effects of

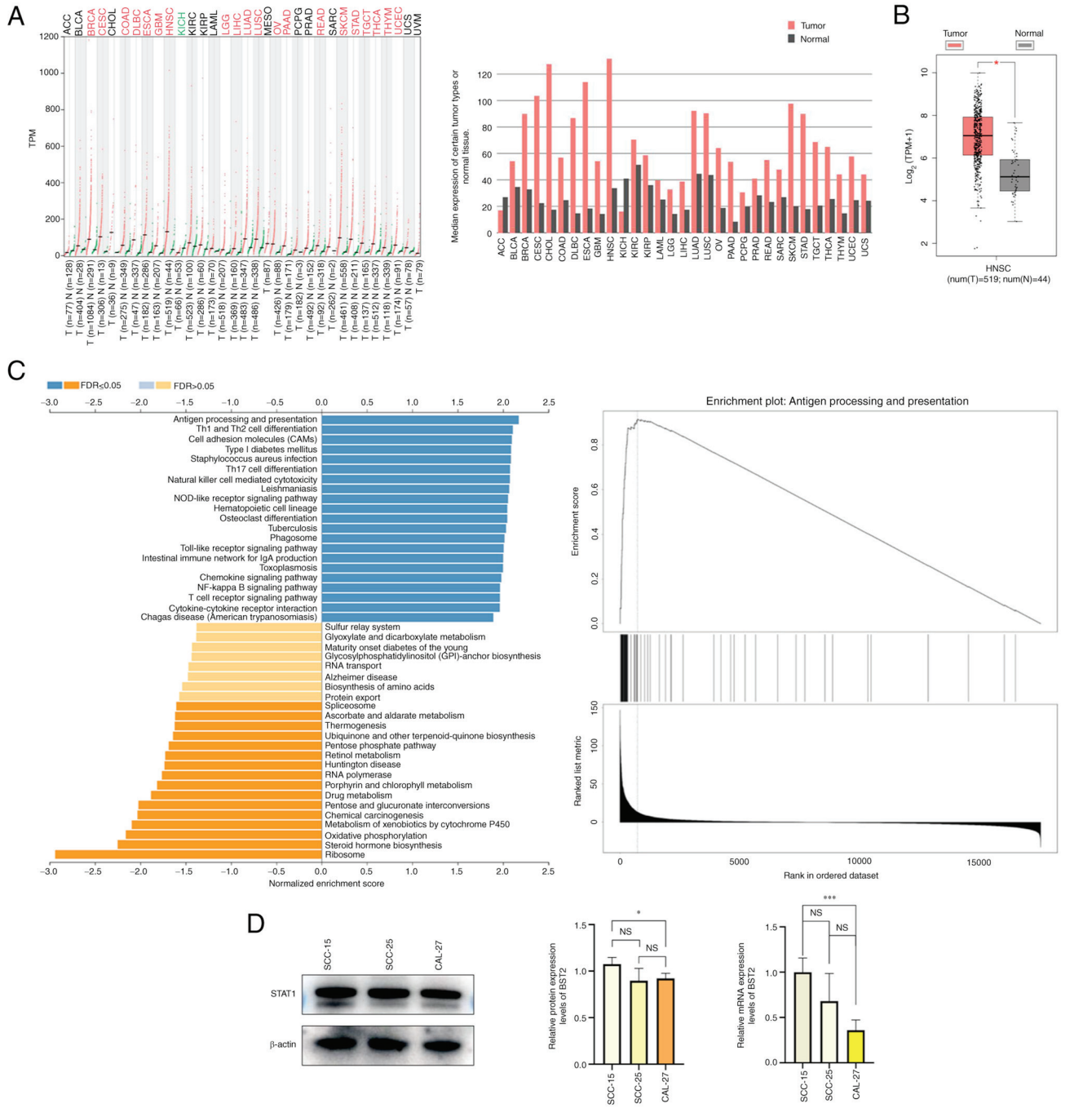

Figure 5. STAT1 is highly expressed in HNSC and OSCC cell lines. (A) The mRNA expression levels of STAT1 from the Gene Expression Profiling Interactive Analysis database in different tumors. (B) Differential expression of STAT1 between normal and tumor tissues (tumor tissues, n=519; normal tissues, n=44). (C) Kyoto Encyclopedia of Genes and Genomes pathway analysis performed using the linkedomics database. (D) The protein and mRNA expression levels of STAT1 in different OSCC cell lines. *P<0.05 and ***P<0.001. HNSC, head and neck squamous cell carcinoma; OSCC, oral squamous cell carcinoma; TPM, transcripts per million; FDR, false discovery rate; NS, not significant; T, tumor; N, normal.

si-STAT1 on the biological behavior of OSCCs were reversed by overexpression of BST2 (Fig. 7B-D).

STAT1 knockdown suppresses proliferation of OSCC via inhibition of the AKT/ERK1/2 signaling pathway in vivo. SCC-15 cells were transfected with si-STAT1or si-NC virus, screened to generate stable clones, and used to construct CDX models using 5-week-old Balb/C nude mice. Excised tumors and tumor growth curves were presented (Fig. 8A). The weight gain and the slope of the growth curve in the si-STAT1 group were greater than those in the si-NC group (Fig. 8A), which indicated that the quality of life of the mice was improved after silencing si-STAT1. Western blotting and RT-qPCR were used to assess the expression of STAT1, BST2, and AKT/ERK1/2 *in vivo*. The protein expression levels of STAT1 and BST2, and the extent of AKT, ERK1/2 and STAT1 phosphorylation were markedly inhibited in the si-STAT1 group compared with the si-NC group (tumors from three representative mice were selected from each group) (Fig. 8B). Furthermore, H&E and IHC staining were performed on the tumor tissues collected from the CDX Model.

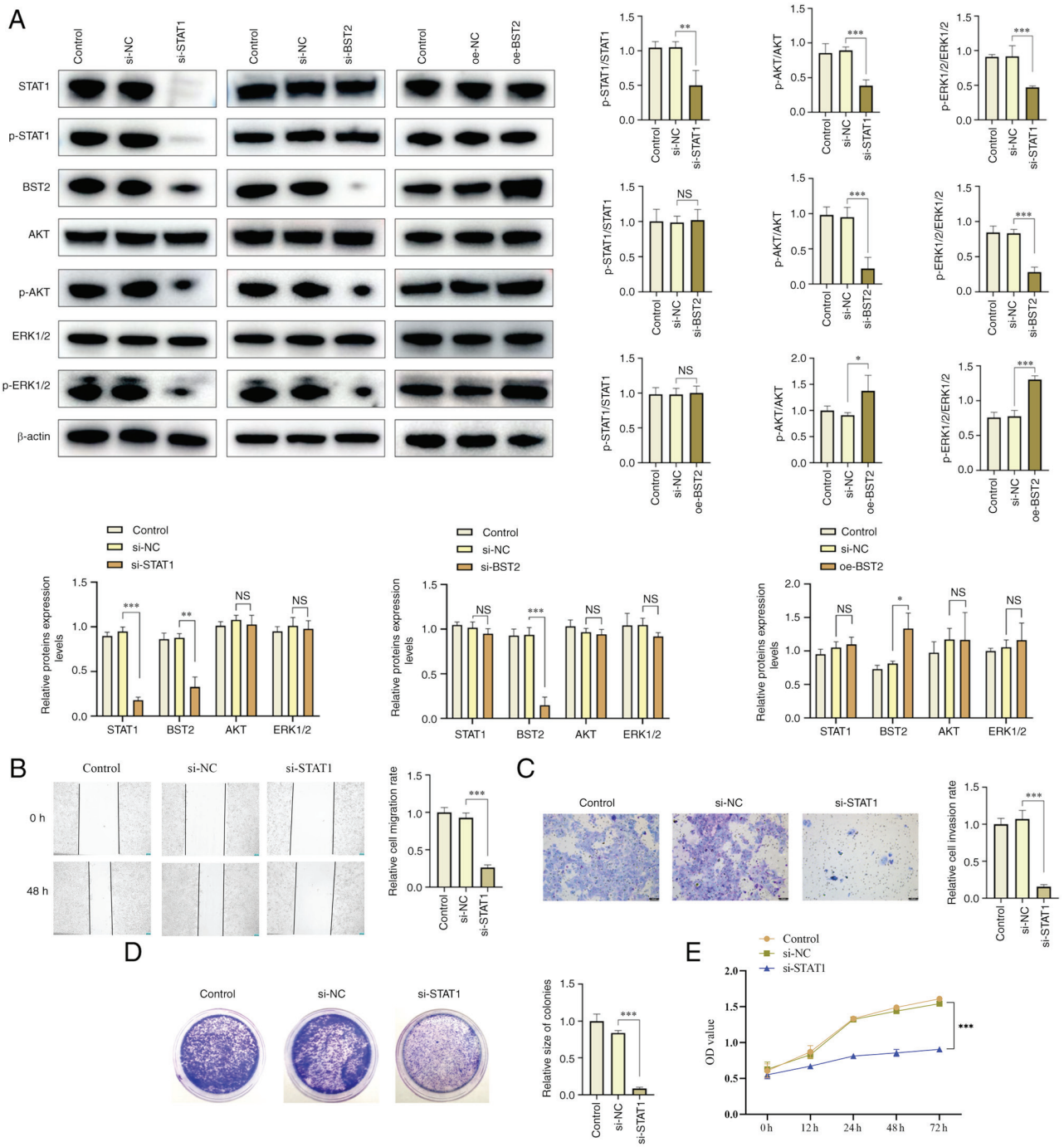

Figure 6. STAT1 positively regulates BST2/AKT/ERK1/2 and biological behavior of OSCC. (A) Western blotting analysis of the protein expression levels of STAT1, BST2, AKT and ERK1/2 and the extent of AKT and ERK1/2 phosphorylation after using si-RNA or oe plasmid to regulate STAT1 or BST2 in SCC-15 cells. (B) Cell scratch test assay (magnification, x50), and (C) Transwell assay (magnification, x100) were used to assess the migration and invasion ability of SCC-15 cells after STAT1 downregulation. (D) Clone formation and (E) cell proliferation assays were performed to assess changes in the viability and proliferation of SCC-15 cells after STAT1 downregulation. *P<0.05, **P<0.01 and ***P<0.001. BST2, bone marrow stromal antigen 2; si, small interfering; oe, overexpression; NC, negative control; p, phosphorylated; NS, not significant.

The data demonstrated that an OSCC model was constructed. In the IHC experiment, the expressions of STAT1, P-STAT1 and BST2 were decreased significantly (Fig. 8C). Which was further demonstrated by the western blotting and RT-qPCR results (Fig. 8D). At the end of the experiment, the lungs and livers of the mice were collected for H&E staining. However, H&E staining demonstrated no metastasis in any of the three groups (S1). It was hypothesized that the period of the animal experiment was too short for the tumors to reach the point of metastasis; however, as the tumors grew in the mice, the tumors reduced the mice's quality of life. Therefore, it was necessary to terminate the experiment at the point chosen and euthanize the mice to avoid excessive tumor growth affecting the quality of life of mice. As all animals were euthanized at the same time, there were no survival curves. One of the mice in the control and si-NC groups was euthanized early due to necrosis and subsequently excluded from analysis; therefore, n=7 in Control and si-NC groups and n=8 in the si-STAT1 group.

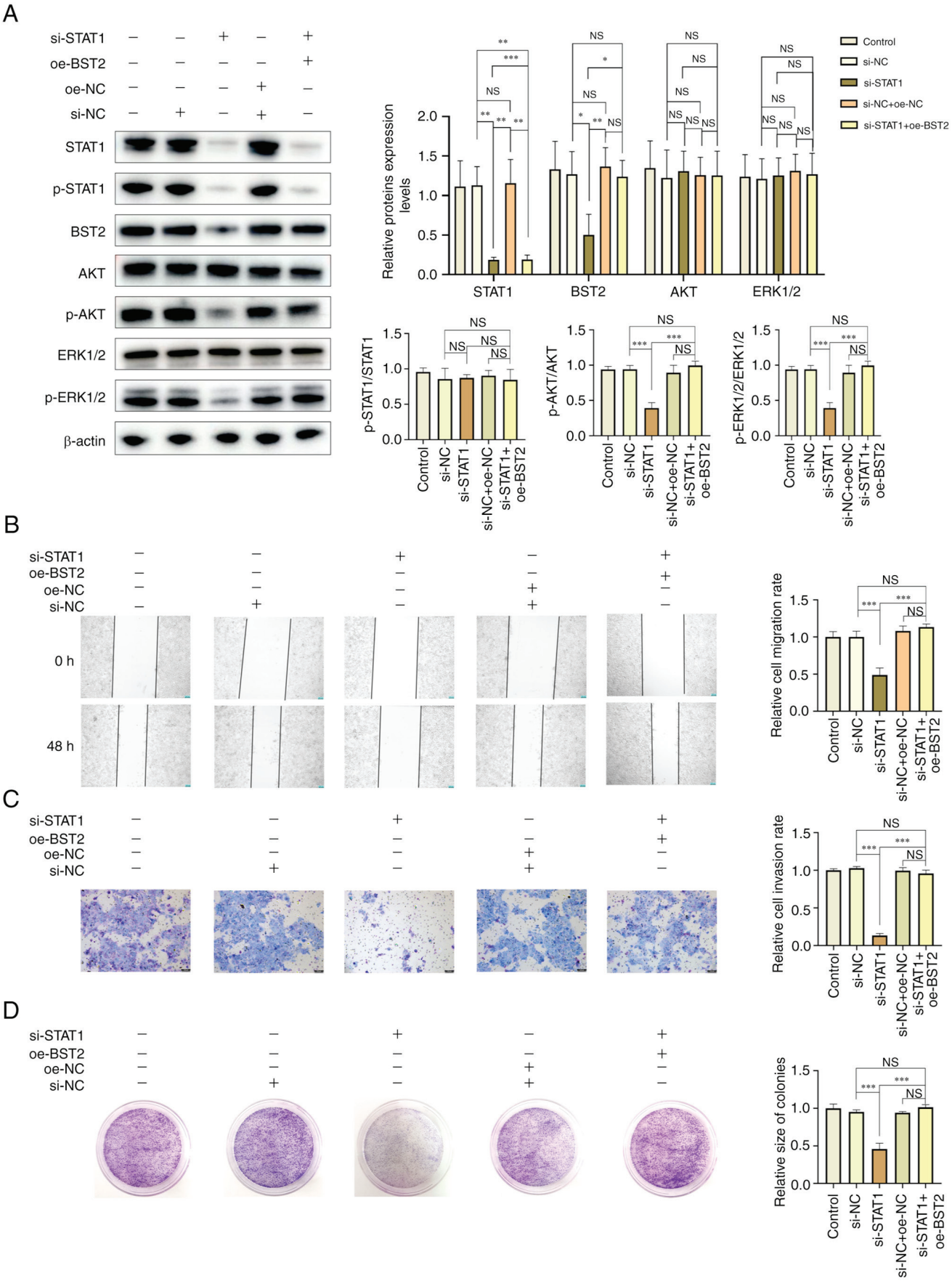

Figure 7. STAT1 and BST2 serve a synergistic role in the biological behavior of oral squamous cell carcinoma. (A) Western blotting analysis of the protein expression levels of STAT1, BST2, AKT, ERK1/2 and the extent of AKT and ERK1/2 phosphorylation after using si-RNA or oe plasmid to regulate STAT1 or BST2 in SCC-15 cells. (B) Cell scratch test assay (magnification, x50), (C) Transwell assay (magnification, x100) and (D) clone formation assay were used to assess the migration, invasion and proliferation of SCC-15 cells after using si-RNA or oe plasmid to regulate STAT1 or BST2. *P<0.05, **P<0.01 and ***P<0.001. BST2, bone marrow stromal antigen 2; si, small interfering; oe, overexpression; NC, negative control; p, phosphorylated; NS, not significant.

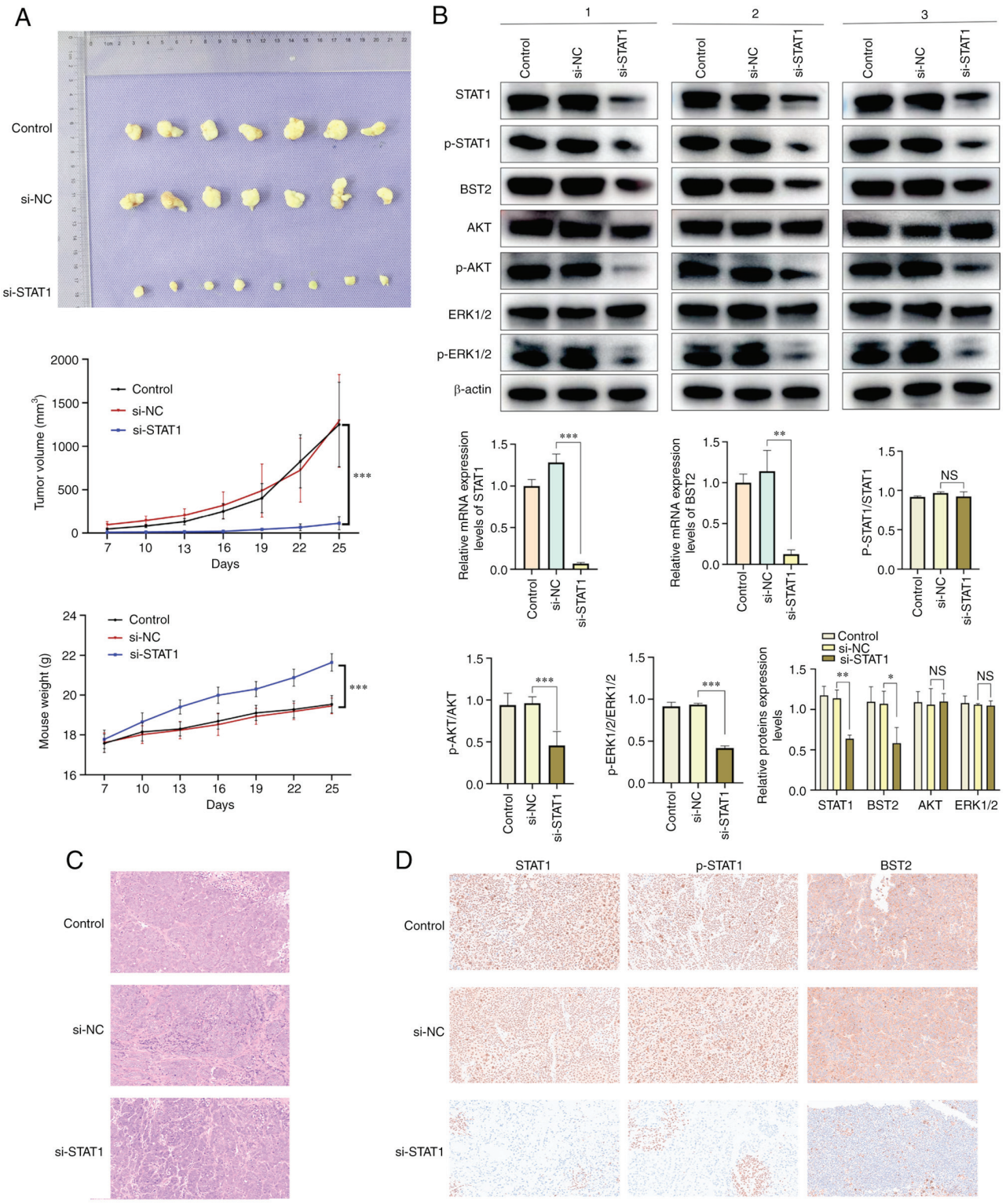

Figure 8. (A) Photograph of tumors excised from mice, growth curve of subcutaneous tumor volume, and the weight of mice. (B) The protein expression levels of STAT1, BST2, AKT and ERK1/2 and the extent of STAT1, AKT and ERK1/2 phosphorylation in vivo after downregulation of STAT1 (n=3 selected from each group) and mRNA expression levels of STAT1 and BST2. Representative images of (C) hematoxylin and eosin and (D) immunohistochemical staining for STAT1, p-STAT1 and BST2 of oral squamous cell carcinoma tumor samples (magnification, x200). *P<0.05, **P<0.01 and ***P<0.001. BST2, bone marrow stromal antigen 2; si, small interfering; oe, overexpression; NC, negative control; p, phosphorylated; NS, not significant.

Discussion

OSCC is a malignant tumor with high morbidity and mortality and is a threat to human health (16). OSCC often involves the tongue and lips, and can easily spread to other organs, including the lungs and lymph nodes (17-19). The lack of specific detection of OSCC tumor boundaries makes it difficult to determine the extent of disease at the time of treatment and often adversely affects a patient's appearance and quality of life after surgery (20). Although

multi-disciplinary therapy, conservation of function surgery and reconstruction of function surgery treatments are available, patients are often at risk of disfigurement and disease recurrence (21,22). Therefore, finding new tumor markers and novel treatment methods for OSCC is very important (23,24).

The present study demonstrated that BST2 was highly expressed in tumors. BST2 is best characterized as an antiviral protein (25), but its role in cancer cannot be ignored. BST2 can act as a tumor-promoting factor in breast cancer (26), but evidence for the role of BST2 in OSCC is lacking. Therefore, the present study was performed to evaluate the role of BST2 as a potential biomarker or therapeutic target in OSCC.

The present study demonstrated that the downregulation of BST2 mRNA and protein expression levels significantly reduced the cell viability, migration, invasion and proliferation of OSCC cells. Increasing the mRNA and protein expression levels of BST2 in OSCC cells significantly increased cell viability, migration, invasion and proliferation. These data indicated that high expression of BST2 has a pro-tumor role in OSCC. Using online tools, it was transcription factors that might regulate BST2 were predicted and it was demonstrated that STAT1 could act as a transcription factor, which bound to a specific sequence in the BST2 promoter region. This prediction was verified using a dual-luciferase reporter assay and led to the evaluation of the role of STAT1 in OSCC.

Members of the STAT family of transcription factors form dimers that translocate from the cytoplasm to the nucleus to act as transcriptional activators, under the stimulation of cytokines and growth factors, such as interferons epidermal growth factor, PDGF and IL6 (27). STAT1, like other STAT family members, dimerizes upon IFN stimulation and translocates to the nucleus where it acts as a transcription factor (28). STAT1 has previously, mainly been studied in breast cancer (29). In breast cancer, STAT1 can be activated by numerous receptors, and it enhances the metastasis, invasion and proliferation of breast cancer cells (30). In the present study, STAT1 was highly expressed in OSCC and acted on the promoter region of BST2 to regulate BST2 expression. Furthermore, the protein and mRNA expression levels of STAT1 were downregulated in OSCC, which demonstrated that knockdown of STAT1 reduced the migration, invasion and proliferation of OSCC cells. The pathways which mediated the interaction between STAT1 and BST2 in OSCC were evaluated.

The AKT/ERK1/2 signaling pathway is vital for cell survival and apoptosis. AKT serves a key role in cell metabolism, apoptosis, cell proliferation and cell migration (31). Furthermore, ERK is activated by phosphorylation and translocated from the cytoplasm to the nucleus, where it mediates the transcriptional activation of upstream factors, and participates in cellular functions, including proliferation, cytoskeleton construction and apoptosis (32). The present study evaluated the signaling pathway through which STAT1/BST2 regulates the biological behavior of OSCC, and demonstrated that STAT1/BST2 acts via the AKT/ERK1/2 signaling pathway. When BST2 and STAT1 expression were altered, corresponding changes were seen in the AKT/ERK1/2 signaling pathway.

To further evaluate the STAT1/BST2/AKT/ERK1/2 signaling pathway, BST2 was overexpressed simultaneously with downregulation of STAT1. When STAT1 was down-regulated, the migration, invasion and proliferation of OSCC cells was significantly decreased. However, simultaneous overexpression of BST2 and STAT1 knockdown restored the AKT/ERK1/2 signaling pathway, and the reduction of OSCC migration, invasion, and proliferation caused by down-regulation of STAT1 was reversed by BST2 overexpression.

To evaluate the role of the STAT1/BST2/AKT/ERK1/2 signaling pathway in OSCC *in vivo*, a CDX model was established using athymic nude mice. The CDX model demonstrated that the growth of tumors in the si-STAT1 group was significantly lower than those in the Control and si-NC groups. This further demonstrated the important role of STAT1/BST2 in OSCC.

Unfortunately, regarding the regulation of the BST2 promoter region by STAT1, while three sequences with high scores were predicted, only one sequence was verified. Therefore, while it was demonstrated that STAT1 can regulate BST2 through the sequence which was assessed, it was not assessed whether the other promoter sequences in the BST2 promoter region could regulate BST2. Therefore, the present study did not demonstrate whether STAT1 can only regulate BST2 through the sequence assessed in the present study. However, this was sufficient to demonstrate that STAT1 can regulate BST2 by regulating its promoter region. Moreover, co-immunoprecipitation experiments were not performed to assess the correlation between STAT1 and BST2 at the protein level, which will need to assessed in future experiments.

Furthermore, it was hypothesized that STAT1 and BST2 are highly expressed in certain cancers where the local immune system where the tumor forms is damaged and, the tumor tissue forms tumor microenvironment with an altered immune system independent of the external environment. Since tumor cells are attacked by the body's immune system, the immune system within tumor tissue may be more active than that of normal tumor tissue (33). This may be a reason why the expression levels of the immune-related proteins STAT1 and BST2 are higher in OSCC than in normal tissues (34-37). Further in-depth research on STAT1 and BST2 in tumor immunity is required.

Few studies have previously reported on role BST2 serves in OSCC. In the present study, STAT1 was identified as an upstream target that controls BST2 expression in OSCC. Furthermore, STAT1 regulated BST2 through the TTT CTGGGAAA sequence to promote the metastasis, invasion and proliferation capability of OSCC. STAT1 is commonly studied in the JAK signaling pathway (38,39); however, the present study demonstrated that STAT1 regulated AKT/ERK signaling by regulating BST2. To the best of our knowledge, the present study is the first to report this finding. STAT1 (40) and BST2 (41) have previously been studied mainly as interferon-stimulated genes.

The present study demonstrated that BST2 is abnormally expressed in OSCC, but the role of BST2 in OSCC has not been elucidated. Given the abnormal expression of BST2 in OSCC, the present study evaluated the regulation of BST2,

determined that STAT1 is a transcription factor that influences BST2 expression, and identified the signaling pathway through which STAT1/BST2 affects the biological behavior of OSCC.

In summary, the present study demonstrated the roles of STAT1 and BST2 in OSCC. Moreover, it was demonstrated that BST2 was regulated by the transcription factor STAT1 and could promote OSCC metastasis, invasion and proliferation via activation of the AKT/ERK1/2 signaling pathway. Immune-related STAT1/BST2 serves an important role in the survival of OSCC. We believe that in the future, we will have a better understanding of the role of the STAT1 and BST2 genes in tumors. Moreover, the combination of this signaling pathway and immunotherapy could become a new target for the treatment of OSCC.

Acknowledgements

We are grateful to Professor Xinxing Wang (Tianjin Institute of Environmental and Operational Medicine) and Professor Gang Chen (The School and Hospital of Stomatology, Tianjin Medical University) for their help with the experiments in this study.

Funding

This work was supported by the National Natural Science Foundation of China (grant nos. 31971106, BWS21L013, 21WS09002 and JK20211A010213).

Availability of data and materials

The datasets used and/or analyzed during the current study are available from the corresponding author on reasonable request.

Authors' contributions

FS, XW and GC were responsible for conception and design. FS and SS were responsible for analysis and interpretation of the data FS drafted the manuscript. XW and GC revised the manuscript critically for intellectual content. FS, XW and GC confirm the authenticity of all the raw data. All authors read and approved the final version of manuscript.

Ethics approval and consent to participate

The overall duration of the animal experiments was 35 days. All animal studies were approved by the Tianjin Institute of Environmental and Operational Medicine Experimental Animal Ethics Committee (approval no. IACUC of AMMS-04-2022-018).

Patient consent for publication

Not applicable.

Competing interests

The authors declare that they have no competing interests.

References

1. Sung H, Ferlay J, Siegel RL, Laversanne M, Soerjomataram I, Jemal A and Bray F: Global cancer statistics 2020: GLOBOCAN estimates of incidence and mortality worldwide for 36 cancers in 185 countries. CA Cancer J Clin 71: 209-249, 2021.
2. Xia C, Dong X, Li H, Cao M, Sun D, He S, Yang F, Yan X, Zhang S, Li N and Chen W: Cancer statistics in China and United States, 2022: profiles, trends, and determinants. Chin Med J (Engl) 135: 584-590, 2022.
3. Sun Z, Sun X, Chen Z, Du J and Wu Y: Head and neck squamous cell carcinoma: Risk factors, molecular alterations, immunology and peptide vaccines. Int J Pept Res Ther 28: 19, 2022.
4. Boldrup L, Coates PJ, Laurell G, Wilms T, Fahraeus R and Nylander K: Downregulation of miRNA-424: A sign of field cancerisation in clinically normal tongue adjacent to squamous cell carcinoma. Br J Cancer 112: 1760-1765, 2015.
5. Chow LQM: Head and Neck Cancer. N Engl J Med 382: 60-72, 2020.
6. Gavrielatou N, Doumas S, Economopoulou P, Foukas PG and Psyrri A: Biomarkers for immunotherapy response in head and neck cancer. Cancer Treat Rev 84: 101977, 2020.
7. Horton JD, Knochelmann HM, Day TA, Paulos CM and Neskey DM: Immune evasion by head and neck cancer: Foundations for combination therapy. Trends Cancer 5: 208-232, 2019.
8. Fan T, Wang X, Zhang S, Deng P, Jiang Y, Liang Y, Jie S, Wang Q, Li C, Tian G, *et al*: NUPR1 promotes the proliferation and metastasis of oral squamous cell carcinoma cells by activating TFE3-dependent autophagy. Signal Transduct Target Ther 7: 130, 2022.
9. Kuang CM, Fu X, Hua YJ, Shuai WD, Ye ZH, Li Y, Peng QH, Li YZ, Chen S, Qian CN, *et al*: BST2 confers cisplatin resistance via NF-κB signaling in nasopharyngeal cancer. Cell Death Dis 8: e2874, 2017.
10. Presle A, Frémont S, Salles A, Commere PH, Sassoon N, Berlioz-Torrent C, Gupta-Rossi N and Echard A: The viral restriction factor tetherin/BST2 tethers cytokinetic midbody remnants to the cell surface. Curr Biol 31: 2203-2213.e5, 2021.
11. Pan XB, Qu XW, Jiang D, Zhao XL, Han JC and Wei L: BST2/Tetherin inhibits hepatitis C virus production in human hepatoma cells. Antiviral Res 98: 54-60, 2013.
12. Cai D, Cao J, Li Z, Zheng X, Yao Y, Li W and Yuan Z: Up-regulation of bone marrow stromal protein 2 (BST2) in breast cancer with bone metastasis. BMC Cancer 9: 102, 2009.
13. Levy DE, Kessler DS, Pine R and Darnell JE Jr: Cytoplasmic activation of ISGF3, the positive regulator of interferon-alpha-stimulated transcription, reconstituted in vitro. Genes Dev 3: 1362-1371, 1989.
14. Knapek KJ, Georges HM, Van Campen H, Bishop JV, Bielefeldt-Ohmann H, Smirnova NP and Hansen TR: Fetal lymphoid organ immune responses to transient and persistent infection with Bovine viral Diarrhea virus. Viruses 12: 816, 2020.
15. Vasaikar SV, Straub P, Wang J and Zhang B: LinkedOmics: Analyzing multi-omics data within and across 32 cancer types. Nucleic Acids Res 46: D956-D963, 2018.
16. Liu J, Jiang X, Zou A, Mai Z, Huang Z, Sun L and Zhao J: circIGHG-induced epithelial-to-mesenchymal transition promotes oral squamous cell carcinoma progression via miR-142-5p/IGF2BP3 signaling. Cancer Res 81: 344-355, 2021.
17. Cao M, Shi E, Wang H, Mao L, Wu Q, Li X, Liang Y, Yang X, Wang Y and Li C: Personalized targeted therapeutic strategies against oral squamous cell carcinoma. An evidence-based review of literature. Int J Nanomedicine 17: 4293-4306, 2022.
18. Chen X, Liu Q, Chen Y, Wang L, Yang R, Zhang W, Pan X, Zhang S, Chen C, Wu T, *et al*: Carboxylesterase 2 induces mitochondrial dysfunction via disrupting lipid homeostasis in oral squamous cell carcinoma. Mol Metab 65: 101600, 2022.
19. Haidari S, Obermeier KT, Kraus M, Otto S, Probst FA and Liokatis P: Nodal disease and survival in oral cancer: Is occult metastasis a burden factor compared to preoperatively nodal positive neck? Cancers (Basel) 14: 4241, 2022.
20. Chen X, Chen DR, Liu H, Yang L, Zhang Y, Bu LL, Sun ZJ and Cai L. Local delivery of gambogic acid to improve anti-tumor immunity against oral squamous cell carcinoma. J Control Release 351: 381-393, 2022.
21. Ju WT, Xia RH, Zhu DW, Dou SJ, Zhu GP, Dong MJ, Wang LZ, Sun Q, Zhao TC, Zhou ZH, *et al*: A pilot study of neoadjuvant combination of anti-PD-1 camrelizumab and VEGFR2 inhibitor apatinib for locally advanced resectable oral squamous cell carcinoma. Nat Commun 13: 5378, 2022.

22. Poell JB, Wils LJ, Brink A, Dietrich R, Krieg C, Velleuer E, Evren I, Brouns ER, de Visscher JG, Bloemena E, *et al*: Oral cancer prediction by noninvasive genetic screening. Int J Cancer 152: 227-238, 2022.
23. de Wit JG, van Schaik JE, Voskuil FJ, Vonk J, de Visscher SAHJ, Schepman KP, van der Laan BFAM, Doff JJ, van der Vegt B, Plaat BEC, *et al*: Comparison of narrow band and fluorescence molecular imaging to improve intraoperative tumour margin assessment in oral cancer surgery. Oral Oncol 134: 106099, 2022.
24. Sun Y, Zhou Q, Sun J, Bi W, Li R, Wu X, Li N, Song L, Yang F and Yu Y: DDX59-AS1 is a prognostic biomarker and correlated with immune infiltrates in OSCC. Front Genet 13: 892727, 2022.
25. Wang SM, Huang KJ and Wang CT: Severe acute respiratory syndrome coronavirus spike protein counteracts BST2-mediated restriction of virus-like particle release. J Med Virol 91: 1743-1750, 2019.
26. Mahauad-Fernandez WD and Okeoma CM: Cysteine-linked dimerization of BST-2 confers anoikis resistance to breast cancer cells by negating proapoptotic activities to promote tumor cell survival and growth. Cell Death Dis 8: e2687, 2017.
27. Yu H, Pardoll D and Jove R: STATs in cancer inflammation and immunity: A leading role for STAT3. Nat Rev Cancer 9: 798-809, 2009.
28. Seidel HM, Milocco LH, Lamb P, Darnell JE Jr, Stein RB and Rosen J: Spacing of palindromic half sites as a determinant of selective STAT (signal transducers and activators of transcription) DNA binding and transcriptional activity. Proc Natl Acad Sci USA 92: 3041-3045, 1995.
29. Wong GL, Manore SG, Doheny DL and Lo HW: STAT family of transcription factors in breast cancer: Pathogenesis and therapeutic opportunities and challenges. Semin Cancer Biol 86: 84-106, 2022.
30. Feng J, Li Y, Zhu L, Zhao Q, Li D, Li Y and Wu T: STAT1 mediated long non-coding RNA LINC00504 influences radio-sensitivity of breast cancer via binding to TAF15 and stabilizing CPEB2 expression. Cancer Biol Ther 22: 630-639, 2021.
31. Gu Y, Wang R, Chen P, Li S, Chai X, Chen C, Liu Y, Cao Y, Lv D, Hong Z, *et al*: In situ synthesis and unidirectional insertion of membrane proteins in liposome-immobilized silica stationary phase for rapid preparation of microaffinity chromatography. Acta Pharm Sin B 12: 3682-3693, 2022.
32. Mao X, Wang X, Jin M, Li Q, Jia J, Li M, Zhou H, Liu Z, Jin W, Zhao Y and Luo Z: Critical involvement of lysyl oxidase in seizure-induced neuronal damage through ERK-Alox5-dependent ferroptosis and its therapeutic implications. Acta Pharm Sin B 12: 3513-3528, 2022.
33. Jeremiah N, Ferran H, Antoniadou K, De Azevedo K, Nikolic J, Maurin M, Benaroch P and Manel N: RELA tunes innate-like interferon I/III responses in human T cells. J Exp Med 220: e20220666, 2023.
34. Ivashkiv LB: IFNγ: Signalling, epigenetics and roles in immunity, metabolism, disease and cancer immunotherapy. Nat Rev Immunol 18: 545-558, 2018.
35. Lau CM, Adams NM, Geary CD, Weizman OE, Rapp M, Pritykin Y, Leslie CS and Sun JC: Epigenetic control of innate and adaptive immune memory. Nat Immunol 19: 963-972, 2018.
36. Yang J, Zhang Q, Wang J, Lou Y, Hong Z, Wei S, Sun K, Wang J, Chen Y, Sheng J, *et al*: Dynamic profiling of immune microenvironment during pancreatic cancer development suggests early intervention and combination strategy of immunotherapy. EBioMedicine 78: 103958, 2022.
37. Cao W and Bover L: Signaling and ligand interaction of ILT7: receptor-mediated regulatory mechanisms for plasmacytoid dendritic cells. Immunol Rev 234: 163-176, 2010.
38. Feketshane Z, Adeyemi SA, Ubanako P, Ndinteh DT, Ray SS, Choonara YE and Aderibigbe BA: Dissolvable sodium alginate-based antibacterial wound dressing patches: Design, characterization, and in vitro biological studies. Int J Biol Macromol 123460, 2023.
39. Zhang Y, Zhang Z, Chen L and Zhang X: Tumor cells-derived conditioned medium induced pro-tumoral phenotypes in macrophages through calcium-nuclear factor κB interaction. BMC Cancer 22: 1327, 2022.
40. Ren X, Wang D, Zhang G, Zhou T, Wei Z, Yang Y, Zheng Y, Lei X, Tao W, Wang A, *et al*: Nucleic DHX9 cooperates with STAT1 to transcribe interferon-stimulated genes. Sci Adv 9: eadd5005, 2023.
41. Gringhuis SI, Kaptein TM, Remmerswaal EBM, Drewniak A, Wevers BA, Theelen B, D'Haens GRAM, Boekhout T and Geijtenbeek TBH: Fungal sensing by dectin-1 directs the non-pathogenic polarization of T_H17 cells through balanced type I IFN responses in human DCs. Nat Immunol 23: 1735-1748, 2022.